Colloids and Surfaces A 583 (2019) 123970

Contents lists available at ScienceDirect

Colloids and Surfaces A

journal homepage: www.elsevier.com/locate/colsurfa

Alginate-cellulose biopolymeric beads as efficient vehicles for encapsulation and slow-release of herbicide

Andressa B. Nörnberg[a], Vinicios R. Gehrke[b], Henrique P. Mota[a], Edinalvo R. Camargo[b], André R. Fajardo[a,*]

[a] Laboratório de Tecnologia e Desenvolvimento de Compósitos e Materiais Poliméricos (LaCoPol), Centro de Ciências Químicas, Farmacêuticas e de Alimentos, Universidade Federal de Pelotas (UFPel), Campus Capão do Leão s/n, 96010-900, Pelotas, RS, Brazil

[b] Departamento de Fitossanidade, Faculdade de Agronomia Eliseu Maciel, Universidade Federal de Pelotas (UFPel), Campus Capão do Leão s/n, 96010-900, Pelotas, RS, Brazil

GRAPHICAL ABSTRACT

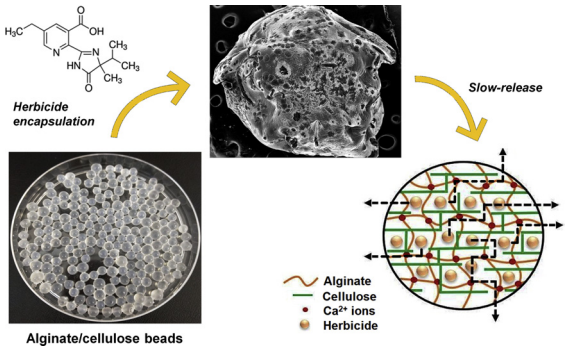

ARTICLE INFO

Keywords:
Alginate
Cellulose
Controlled release
Imazethapyr
Release kinetic models
Tortuosity effect

ABSTRACT

Alginate (ALG) and alginate/cellulose (ALG/CEL) beads were prepared and tested as potential vehicles for encapsulation and controlled release of imazethapyr (IMZ), a broad spectrum herbicide. The incorporation of a small amount of CEL (5 w/w-%) into the ALG network allowed to increase the encapsulation efficiency of IMZ (> 85%). CEL also contributed to control of some important features such as the effect of pH on the liquid uptaking and stability in water. Release profile of IMZ from the prepared beads (ALG@IMZ and ALG/CEL@IMZ) was assessed in water, and it revealed that these carrier devices behaved as slow release formulations as compared to pure IMZ. Moreover, CEL-containing beads reduced the release of IMZ more efficiently than the pristine ALG beads. The release profiles of both carrier systems were well fitted by the Korsmeyer-Peppas model, which indicated that in both cases the IMZ release is driven by Fickian diffusion mechanism. The time taken for 50% of IMZ to be release was 11.30 days for ALG beads, while for the ALG/CEL beads this time was increased to 43.73 days. The experimental performance presented by ALG and ALG/CEL beads demonstrated that both systems could control and prolong the release of IMZ, which is paramount for their practical application as slow-release systems.

* Corresponding author.
E-mail address: andre.fajardo@pq.cnpq.br (A.R. Fajardo).

https://doi.org/10.1016/j.colsurfa.2019.123970
Received 17 August 2019; Received in revised form 11 September 2019; Accepted 11 September 2019
Available online 12 September 2019

1. Introduction

One of the most significant challenges faced by modern crop producers is to reduce herbicides use to fit many economic, environmental, and health reasons. Although the use of the herbicides had been essential to the development of agriculture in the last century, their widespread and intensive use in various crops may cause environmental issues such as soil and hydric bodies (surface and groundwater) contamination [1,2]. By consequence, residual herbicides (in the environment and edible products) may also cause harmful side effects for the plant, animal, and human health [1,3]. In parallel, the use of excessive amounts of herbicides can be justified due to the loss of efficiency caused by some internal and external factors. For example, some herbicides show low chemical stability (i.e., photo or biodegradability) or are lost through soil-herbicide binding (adsorption), leaching, and volatilization [4,5]. According to some studies, a significant part of the herbicide used in the field crops (> 90%) never reaches its target to produce the desired response at the precise time and in quantity required [6]. An alternative extensively studied to mitigate these two main issues (i.e., excessive use and loss of efficiency) is associated with the use of delivery devices to protect and control the release rate of herbicides in the field crops [7,8]. In light of this, herbicides molecules can be chemically or physically bound to clay minerals, silica, coal, or polymers or embedded into capsules-type devices (micro or nanoparticles, micelles, gels, and others) prepared from natural or synthetic polymers [9–12]. Currently, composite materials made from the mixture of polymers with other kinds of materials (mainly clay minerals) have also been investigated primarily as delivery devices [13,14].

In this study, microspheres, commonly referred to as beads, were prepared from sodium alginate (SA) ionically crosslinked by divalent calcium ions (Ca^{2+}). Alginates are polysaccharides naturally present in brown seaweed cell walls that are commercially extracted in their sodium form because of their solubility in cold water. From a molecular viewpoint, SA is a linear binary copolymer consisting of (1→4)-linked residues of β-D-mannuronic acid (M units) and α-L-guluronic acid (G units), where the M/G ratio has a substantial effect on its physicochemical properties [15]. This polysaccharide is widely used in various industrial segments such as textile, food, paper, biomedical, and pharmaceutical and cosmetic because of their gelling, viscofiying, and stabilizing properties [16,17]. Moreover, SA also exhibits other attractive properties like biodegradability, biocompatibility, low toxicity, natural abundance, and low-cost production [15,16]. Considering these aspects, the use of SA to design delivery devices to herbicides is highly attractive [18–20]. Herein, cellulose microfibers (CEL) isolated from rice husks, an agricultural residue, were incorporated into conventional alginate-Ca^{2+} beads to enhance the encapsulation efficiency of an herbicide model and, also, to control their release rate. Cellulose is a linear polysaccharide consisting of β(1→4)-linked D-glucose units and is the major component of plant cell walls. Although cellulose is insoluble in water; it is a biodegradable, biocompatible, and non-toxic compound widely used in different industries [21]. Up to date, composite materials based on alginate/cellulose were not investigated as herbicide delivery systems. Imazethapyr (IMZ), an imidazole compound, was used as an herbicide model. IMZ is used as a selective herbicide utilized for broad-spectrum control of leaf weed and grasses in soybean and leguminous crops [22,23]. For example, IMZ is commonly used to control red rice in irrigated rice crops. Few studies report on the encapsulation of IMZ into polymeric devices as well as its release profile. Thus, the present study investigates the potential of alginate and alginate/cellulose beads to encapsulate and control the release of IMZ.

2. Experimental section

2.1. Materials

Alginic acid sodium salt (SA) from brown algae with a medium viscosity (approximate M/G ratio of 1.56 and M_w range of 80–120 kDa) was purchased from Sigma-Aldrich (USA). Calcium chloride ($CaCl_2$, P.A.) and was purchased from LabSynth (Brazil). Cellulose microfibers (CEL) were isolated from rice husks donated by a local rice mill (Pelotas-RS, Brazil), according to the protocol described by Voss et al. [24] Imazethapyr (IMZ) technical grade was kindly donated by Adama S/A (Brazil). These chemicals were used as such without further purification.

2.2. Preparation of ALG and ALG/CEL beads

Alginate beads (ALG) were prepared by the ionotropic gelation method, using $CaCl_2$ as the crosslinking agent. Briefly, SA (600 mg) was solubilized in distilled water (30 mL) under magnetic stirring (300 rpm) at room temperature for 4 h. Then, the resulting solution was transferred to a plastic syringe equipped with a needle (internal diameter of 1.0 mm) and carefully added dropwise (speed 1 mL min^{-1}) into $CaCl_2$ solution (5 w/v-%, 100 mL), which was kept under mild orbital stirring (˜100 rpm) to form spherical-like beads. The as-formed ALG beads were left to harden in $CaCl_2$ solution for 3 h at room temperature under orbital stirring (100 rpm). Next, the beads were thoroughly washed with distilled water (˜500 mL) to eliminate the excess of ions and, then, ovendried at 40 °C for 48 h.

In parallel, ALG beads containing CEL (denoted as ALG/CEL) were prepared using a similar protocol with minor modifications. Herein, 30 mg of CEL was added to the SA solution (600 mg in 30 mL of distilled water) under vigorous stirring (1000 rpm for 6 h) before the dropwise step. The SA/CEL mass ratio was fixed 1:0.05 considering previous experiments. Under these experimental conditions, the dispersion of CEL on SA solution was inefficient when higher amounts of CEL were utilized.

2.3. Preparation of beads loaded with IMZ

Beads loaded with IMZ were prepared using the same protocol described in Section 2.2. However, specific amounts of IMZ (5, 10, 15 or 20 w/w-% in respect to the total mass of polysaccharides) were added to the alginate or alginate/cellulose solutions before the dropwise process. The as-prepared beads (denoted as ALG@IMZ or ALG/CEL@IMZ) were collected, while LC–MS/MS technique analyzed the remaining $CaCl_2$ solutions to determine the residual amounts of IMZ. From these data, the loading capacity (LC-%) and encapsulation efficiency (EE-%) for each tested condition were calculated per Eqs. (1) and (2) [25]:

$$LC = \left[\frac{amount\ of\ encapsulated\ IMZ}{total\ bead\ weight}\right] \times 100\% \quad (1)$$

$$EE = \left[\frac{(initial\ amount\ of\ IMZ - amount\ of\ IMZ\ free\ in\ solution)}{initial\ amount\ of\ IMZ}\right] \times 100\% \quad (2)$$

2.4. Characterization

Fourier transform infrared (FTIR) analyses were done in a Shimadzu (model IR-Affinity-1, Japan) spectrometer operating in the spectral region of 4000–400 cm^{-1} at 4 cm^{-1} resolution, employing conventional KBr pellet method. X-ray diffraction (XRD) patterns were obtained in a Siemens (model D-500, Germany) diffractometer using a Cu-K_α radiation source at a voltage of 30 kV and current of 20 mA. Before

each analysis, the samples were milled using an Anton Parr (model BM500, USA) ball mill equipment. After that, diffraction patterns were recorded at a scan rate of 4° min^{-1} in a 2θ range of 10° to 70°. Thermogravimetric analysis (TGA) was done in a Shimadzu Analyzer (model DTG60, Japan) with a scanning rate of 10 °C min^{-1} under $N_{2(g)}$ atmosphere with a flow of 20 mL min^{-1} in a range of temperature of 25–600 °C. Microscopic images were taken using a scanning electron microscope (SEM) Jeol (model JSM-6610LV, Japan) using an acceleration voltage of 8–10 kV. Before the SEM visualization, the surface of the samples was sputtered with a thin gold coat. For quantitative analyses, liquid chromatography coupled with mass spectrometry was employed using an HPLC-ESI-MS/MS (Thermo Scientific, model Q-Exactive Focus hybrid quadrupole-Orbitrap MS, USA). At optimized conditions, a volume of 10 µL of each sample was injected at 40 °C, while the total run time was 5 min (an equilibrium time of 1 min was allowed before the next injection). The chromatographic separation was done using a Thermo Scientific column (model Accucuore XL C18, 4 µm, 150 x 4.6 mm) at a 0.25 mL min^{-1} mobile phase flow rate. Mobile phase A was ultrapure water containing 0.1% of formic acid and 5 mM ammonium formate, and B was 100% methanol. The solute detection was done by MS/MS spectroscopy considering the appearing of fragment ion *m/z* 290.14992. Triplicates were done for each sample (n ≈ 3). The point of zero charge (PZC) values for the prepared beads were examined in 0.1 mol L^{-1} NaCl solutions at room temperature. For this, samples (30 mg) were put in vials filled with NaCl solution (50 mL) and, then, the initial pH value was adjusted (2–12) with 0.1 mol L^{-1} HCl or 0.1 mol L^{-1} NaOH solutions using a Hannah Instruments (model HI2211, USA) pHmeter. All vials were stirred using an orbital shaker (150 rpm) for 24 h. Later, the final pH of each system was measured carefully. The differences between the final and the initial pH values (ΔpH) were then plotted against the initial pH values. The PZC values were estimated from the points where the initial pH at which ΔpH is zero [26].

2.5. Swelling experiments

2.5.1. Effect of different pH conditions

Swelling experiments assessed the effect of the pH of the medium on the liquid uptake behavior of the prepared beads containing IMZ. Thus, samples (30 mg) were put in vials filled with distilled water and, then, the pH was adjusted to 5, 6 or 7 using HCl or NaOH solutions (0.1 mol L^{-1}). The samples were kept immersed in the swelling medium at room temperature. At pre-determined time intervals, the swollen beads were collected, the excess of surface liquid was carefully removed, and they were weighed. This procedure was done in triplicate for each sample. The swelling rate after each time interval was calculated per Eq. (3):

$$Swelling\ (\%) = \left[\left(\frac{swollen\ weight\ of\ beads}{dry\ weight\ of\ beads}\right) - 1\right] \times 100\% \quad (3)$$

2.5.2. Stability in water

The stability of the prepared beads in water was assessed by *in vitro* experiments done in triplicate. Briefly, dry beads samples (30 mg) were put in vials filled with water (50 mL, pH 6) at room temperature. The set (vials + beads) was stirred using an orbital shaker (100 rpm) for four weeks and, then, the beads were recovered and oven-dried up to a constant weight. Later, the samples were reweighed. The degradation percentage after this while was calculated per Eq. (4):

$$Degradation\ (\%) = \left[\frac{initial\ beads\ weight\ -\ dry\ beads\ weight\ after\ soaking\ period}{initial\ beads\ weight}\right] \times 100\% \quad (4)$$

2.6. Release experiments

In vitro experiments for releasing IMZ from ALG@IMZ and ALG/CEL@IMZ were performed using distilled water as the release medium at room temperature under mild stirring (50 rpm). In conical flasks, 200 mg of beads were immersed in 250 mL of distilled water (pH 6). Later, aliquots of 1.0 mL were withdrawn from each flask periodically and, then, subjected to IMZ determination by LC–MS/MS analysis. It is worthy to say that each aliquot sample withdrawn was replaced with the same volume of fresh solution. The releasing profile of IMZ (not encapsulated) was also investigated under similar experimental conditions. In this case, 30 mg of pure IMZ was added to the releasing media (distilled water, pH 6). Again, each experiment was done in triplicate. The following equation calculated the percentage of IMZ released after each time interval:

$$IMZ\ released = \left[\frac{amount\ of\ IMZ\ in\ solution}{amount\ of\ IMZ\ encapsulated}\right] \times 100\% \quad (5)$$

3. Results and discussion

3.1. Characterization

Table 1 presents the LC-% and EE-% values calculated for the different ALG@IMZ and ALG/CEL-IMZ formulations. For both cases, the LC-% values increased as increased the amount of IMZ; however, the highest EE-% values were obtained for moderate amounts of IMZ. For instance, ALG@IMZ beads prepared with 10 w/w-% of IMZ showed an EE-% of 74.9%, while the ALG/CEL@IMZ beads prepared with 15 w/w-% of IMZ showed an EE-% of 85.6%. The higher encapsulation efficiency presented by the CEL-containing beads containing may result from two hypothesis: (i) the presence of CEL microfibers reduces the crosslinking density within the beads network, which favors the IMZ encapsulation due to availability of empty spaces into the beads, and (ii) the CEL microfibers may interact with the IMZ molecules keeping them into the beads. From these results, ALG@IMZ beads prepared with 10 w/w-% of IMZ and the ALG/CEL@IMZ prepared with 15 w/w-% of IMZ were selected for the further experiments and characterization.

The chemical nature of beads prepared in this work as well as their precursor materials were characterized by FTIR analyses (Figs. 1a,b). The spectrum of pure IMZ presented characteristics bands at 3244 cm^{-1} (OH− stretching), 3050 cm^{-1} (NH− stretching), 2965 cm^{-1} (C–H stretching), 1742 cm^{-1} (CO═ stretching of −COO- group), 1649 cm^{-1} (CN═ stretching), 1556 cm^{-1} (NH− bending, amide group), and 1046 cm^{-1} (NH− out-of-plane bending) corroborating with prior studies [22]. The SA spectrum (Fig. 1a) exhibited a broadband centered at 3433 cm^{-1} (OH− stretching), bands in 2925–2865 cm^{-1} region (C–H stretching of aliphatic CH_x groups), bands at 1632 cm^{-1} and 1417 cm^{-1} due to the CO═ asymmetric and symmetric stretching (−COO- group), and bands in 1100–1030 cm^{-1} region assigned to the COC, CC, and CO−−−−H stretching of pyranose ring [27]. The FTIR

Table 1
Loading capacity (LC-%) and encapsulation efficiency (EE-%) of different ALG@IMZ and ALG/CEL@IMZ formulations.

Samples	Amount of IMZ (w/w-%)[a]	LC-%	EE-%
ALG@IMZ	5	3.2 ± 0.1	66.1 ± 2.2
	10	7.5 ± 0.7	74.9 ± 0.8
	15	9.0 ± 0.3	72.4 ± 1.2
	20	12.4 ± 0.2	71.8 ± 1.6
ALG/CEL@IMZ	5	3.1 ± 0.1	70.2 ± 2.1
	10	7.4 ± 0.2	83.3 ± 1.1
	15	11.9 ± 0.3	85.6 ± 2.8
	20	14.5 ± 0.1	84.0 ± 1.0

[a] Percentage of IMZ mass in respect to the total mass of polysaccharides.

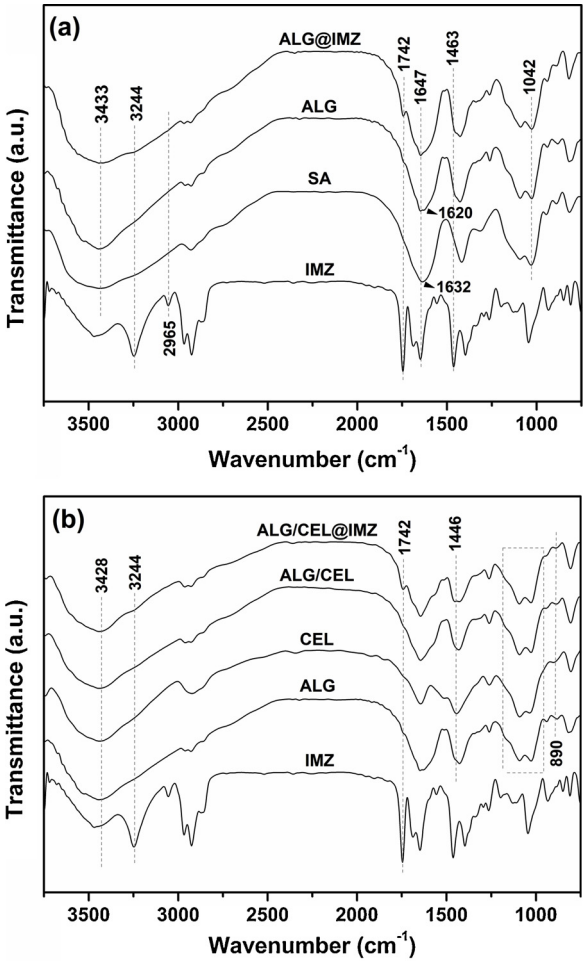

Fig. 1. FTIR spectrum recorded of (a) IMZ, SA, ALG, and ALG@IMZ and (b) IMZ, ALG, CEL, LG/CEL, and ALG/CEL@IMZ.

spectrum of the ALG beads exhibited the characteristics bands of alginate with some discrepancies. For instance, the bands associated with the C═O asymmetric and symmetric stretching vibration were shifted to different wavenumber regions (1620 and 1450 cm^{-1}, respectively) due to the replacement of Na^{+} ions in the uronic acid residue of SA by Ca^{2+} ions [28]. Moreover, the broadband assigned to the O—H stretching (3600–3100 cm^{-1} region) is sharpened in the ALG spectrum suggesting the decrease of the intra and intermolecular hydrogen bonds of alginate due to the Ca^{2+}-mediated crosslinking process and egg-box structure formation [28]. The spectrum recorded for the IMZ loaded beads (ALG@IMZ) exhibited the bands proceeding from ALG added with characteristics bands of IMZ (3244 cm^{-1} and 1742 cm^{-1}) confirming the encapsulation of the herbicide within the alginate-Ca^{2+} network (see Fig. 1a).

Fig. 1b displays the FTIR spectra recorded for the beads prepared with CEL. As observed, the spectrum of pure CEL exhibited a broadband centered at 3428 cm^{-1} (OH— stretching), bands at 2918 cm^{-1} (C–H stretching), 1612 cm^{-1} (OH— bending due to adsorbed water molecules), 1446 cm^{-1} (CH_2 asymmetric bending), 1320 cm^{-1} (CH_2 wagging bending), bands in the 1100–1040 cm^{-1} region due to COC, CC, and CO————H stretching, and a small band at 890 cm^{-1} assigned to the β-glycosidic linkages between the glucose units of CEL [29]. The spectrum of ALG/CEL beads exhibited slight discrepancies as compared to the ALG spectrum likely due to the structural similarity between these two polysaccharides. The low amount of CEL used to prepare the bands may contribute to this scenery too. Only the bands associated with the hydroxyl groups (e.g., O—H and CO—H) exhibited some changes, which can be ascribed to the interaction between the ALG and

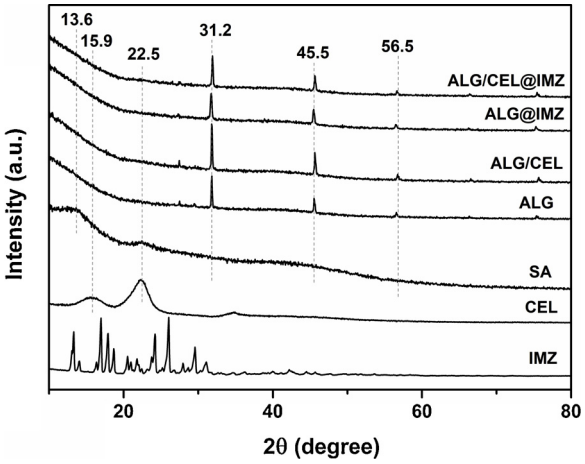

Fig. 2. XRD patterns recorded of IMZ, SA, CEL, ALG, ALG/CEL, ALG@IMZ, and ALG/CEL@IMZ.

CEL by hydrogen bonding. It is worthy to note that the band 890 cm^{-1} is evident in the ALG/CEL spectrum, indicating that CEL is entrapped into the ALG network. Again, the spectrum of ALG/CEL@IMZ exhibited the ALG/CEL bands added with the bands proceeding from IMZ (3244 cm^{-1} and 1742 cm^{-1}) confirming its encapsulation.

The structure of the prepared beads was investigated by XRD analysis, and the diffraction patterns are shown in Fig. 2. The XRD pattern of pure IMZ exhibited many well-defined diffraction peaks in the 2θ range between 13–31° suggesting a crystalline arrangement for this compound. The XRD pattern of SA shows two peaks at 2θ ≈ 13.6° and 22.5°, which are ascribed to the reflection of their (110) plane from G-units and (200) plane from M-units [30]. After the crosslinking with Ca^{2+} ions, the diffraction peaks of alginate disappeared, which indicate that this process affected the crystalline arrangement of SA. In contrast, the XRD pattern of ALG beads presented diffraction peaks at 2θ ≈ 31.2°, 45.5°, and 56.5°, which are associated with the egg-box structure, a large junction zone formed due to the crosslinking of the alginate chains with Ca^{2+} ions [31,32]. The XRD pattern of ALG@IMZ exhibited only the diffraction peaks proceeding of ALG structure. The absence of the characteristic diffraction peaks of IMZ, in this case, indicates that the encapsulation of the herbicide within the ALG beads converted it to an amorphous state. Probably, interaction forces between ALG network and IMZ impaired the crystallization process after the encapsulation procedure. Apart from this, the absence of new diffraction peaks as compared to ALG pattern suggests that the encapsulation of IMZ does not affect the alginate-Ca^{2+} structure. Considering the XRD analyses performed with the CEL containing beads (Fig. 2), the XRD pattern of pure CEL exhibited the characteristic diffraction peaks of cellulose type I structure (2θ ≈ 15.9°, 22.3°, and 34.2°), which are associated with the reflection planes (1–10), (200), and (004), respectively [29,33]. These peaks were not observed in the XRD patterns recorded from ALG/CEL and ALG/CEL@IMZ, likely due to the low amount of CEL incorporated into the ALG network or to the interaction between CEL-ALG that can affect the crystallinity of cellulose [34]. Similarly to the ALG@IMZ beads, the characteristic diffraction peaks of IMZ were not observed in the XRD pattern of ALG/CEL@IMZ confirming that after encapsulation, the herbicide was converted to the amorphous state.

The thermal stability of the prepared beads was investigated by TGA/DTG analyses (Fig. 3a and b), which demonstrated that pure IMZ shows only one weight loss stage between 215 °C to 300 °C with a maximum at 263 °C corresponding to its thermal degradation (˜90% of weight loss). The TGA curve of SA exhibited two weight loss stages, where the first has a maximum near 67 °C due to the loss of volatile compounds and water (˜14% of weight loss) and the second between 210 °C to 290 °C with a maximum at 243 °C due to the thermal depolymerization accomplished by the degradation of the alginate backbone

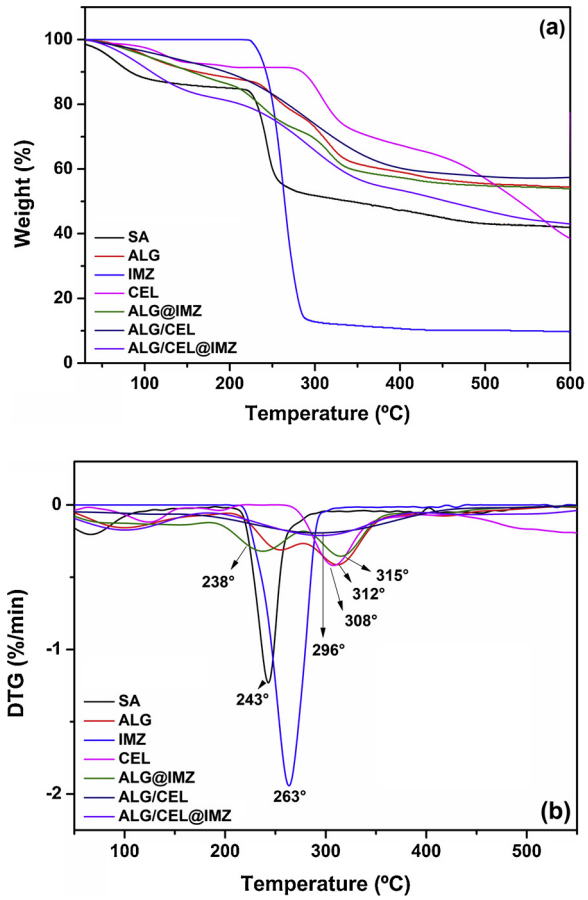

Fig. 3. (a) TGA and (b) DTG curves recorded of SA, IMZ, ALG, ALG/CEL, ALG@IMZ, and ALG/CEL@IMZ.

(˜43% of weight loss) [35]. After the crosslinking with Ca^{2+} ions, the TGA curve of ALG beads revealed that the thermal depolymerization of the alginate (˜33% of weight loss) occurred on a broader temperature range (200–370 °C) with two maximum peaks at 256 °C and 312 °C. The appearing of these two distinct peaks can be associated with the depolymerization of the free chains of alginate occurring at lower temperatures, while the junction zones that result from the egg-box structure are depolymerized at higher temperatures. Moreover, the residue at 600 °C (˜54%) is notoriously more elevated than the residue of SA at the same temperature likely due to the presence of calcium in ALG composition. Apart from this, after the encapsulation of IMZ, the thermal profile of ALG@IMZ was quite similar to that presented by ALG. It was noticed that the peak at 256 °C for ALG was shifted to lower temperature range (maximum at 238 °C) suggesting that IMZ molecules may reduce the intermolecular interactions among the free moieties of the alginate reducing their thermal stability.

In parallel, the TGA/DTG curves obtained to the beads prepared with CEL (Figs. 3a and 3b), indicated that pure CEL has three weight loss stages. The first stage, associated with the water volatilization, occurred in the temperature range of 70–150 °C with a maximum at 124 °C (˜9% of weight loss). The second and third stages occurred in a wide temperature range (170–400 °C) and they can be ascribed to the depolymerization accomplished by the decomposition of small hemicellulose residues (maximum at 195 °C and ˜18% of weight loss) and cellulose (maximum at 308 °C and ˜39% of weight loss) [36]. The differences regarding the chemical nature and structure of hemicellulose and cellulose explain this thermal behavior. The TGA curve of ALG/CEL was completely different as compared to the ALG curve since only two weight losses were noticed. The first, due to the water volatilization, had a maximum near 120 °C (˜10% of weight loss), while the second one occurred in the temperature range of 170–435 °C (˜34% of weight loss). In this case, only one maximum peak at 291 °C was noticed likely due to the overlapping of the peaks associated with the individual systems (ALG network and CEL). The residue at 600 °C was ˜57% for ALG/CEL, a little bit higher than the residue of pristine ALG at this same temperature. According to Figs. 3a and b, is clear that the presence IMZ within the ALG/CEL beads altered the rate of each weight loss stage without changing the temperature range in which they occur. For instance, the weight loss associated with water volatilization was ˜20% (maximum peak at 102 °C), while the weight loss ascribed to the depolymerization/decomposition of the ALG/CEL matrix was ˜45% (maximum peak at 296 °C). From this result, it can be suggested that the IMZ molecules contribute positively to accelerate the thermal degradation of the ALG/CEL beads. The presence of IMZ into the polymeric system may reduce the interactions forces between the ALG and CEL, which impair the thermal stability of the system.

Figs. 4a-d shows digital photographs taken from the as-prepared beads (ALG, ALG@IMZ, ALG/CEL, and ALG/CEL@IMZ). As noticed, all of them showed a spherical shape, which is typically observed for alginate-Ca^{2+} beads prepared via dripping method [37]. Differently, from the ALG, the beads containing CEL showed a whitish color indicating the presence of polysaccharide. As can be seen, the presence of IMZ into both types of beads seems not to change their visual aspect. Furthermore, the size distribution of all beads was different, as demonstrated in Fig. 5.

In general lines, the incorporation of CEL and IMZ within the ALG network increased the average size of the beads. As assessed, the beads size at swollen state can be ordered as follows: ALG/CEL@IMZ (4.31 ± 0.02 mm) > ALG/CEL (4.02 ± 0.08 mm) > ALG@IMZ (3.88 ± 0.01 mm) > ALG/CEL@IMZ (3.54 ± 0.01 mm).

The topography and morphology of the beads were investigated by SEM images taken from their surface region (Figs. 6a-d). All samples presented spherical morphology with some irregularities and high roughness, which is typical of alginate-Ca^{2+} beads. The incorporation of CEL into the ALG network caused slight changes on the beads morphology; it may confirm that the microfibers are confined preferentially into the bulk phase. After the encapsulation of IMZ into the beads, some dark spots randomly distributed on the surface of the bead were observed (see Figs. 6b,d). These spots can be associated with the presence of some IMZ molecules encapsulated on the surface region of the beads [38]. The light contrast between these dark spots and the continuous phase (ALG network) can be ascribed to the difference of electronic density between them.

The development of devices for controlled release of any solutes has to attempt to the surface properties of such devices since the surface region has an enormous effect on their overall efficiency. One of the most important features of the surface of the bead is their charge, which may exert influence on their swelling behavior and trigger the solute release. Considering this, here we assessed the pH_{PZC} for all prepared beads. The pH_{PZC} is denoted as the pH at which the surfaces of the beads are globally neutral. In other words, at pH_{PZC} the number of positive species is equivalent to the number of negative species. Below this pH, the surfaces of the beads are charged positively while beyond this pH, the surfaces are charged negatively. Fig. 7 shows the pH_{PZC} values estimated for each beads sample. The pristine beads (ALG and ALG/CEL) exhibited close values of pH_{PZC} (6.26 and 6.23, respectively), which indicates that the CEL microfibers are restricted to the bulk phase of the beads and exert a negligible effect on the surface region.

In contrast, the encapsulation of IMZ into the beads caused a noticeable change in the pH_{PZC} values. For both systems, ALG@IMZ and ALG/CEL@IMZ, the pH_{PZC} was shifted to low values (4.72 and 4.62) indicating that the loaded beads exhibit a more negative surface. Although IMZ shows an amphoteric nature due to its acidic (carboxylic) and basic (pyridine nitrogen) functional groups under the experimental conditions (pH ˜6) it shows a negative charge density caused by the deprotonation of its carboxylic groups (pKa ˜3.9) [39]. The presence of

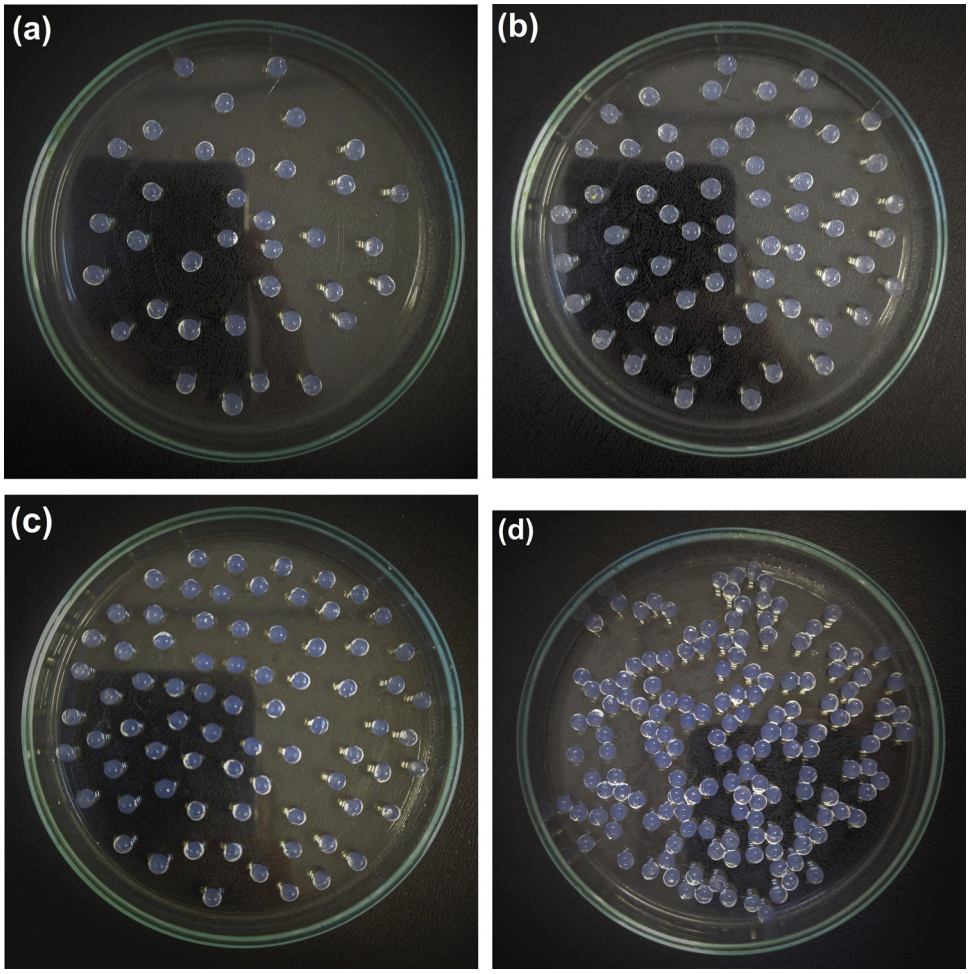

Fig. 4. Photographic images of (a) ALG, (b) ALG@IMZ, (c) ALG/CEL, and (d) ALG/CEL@IMZ beads.

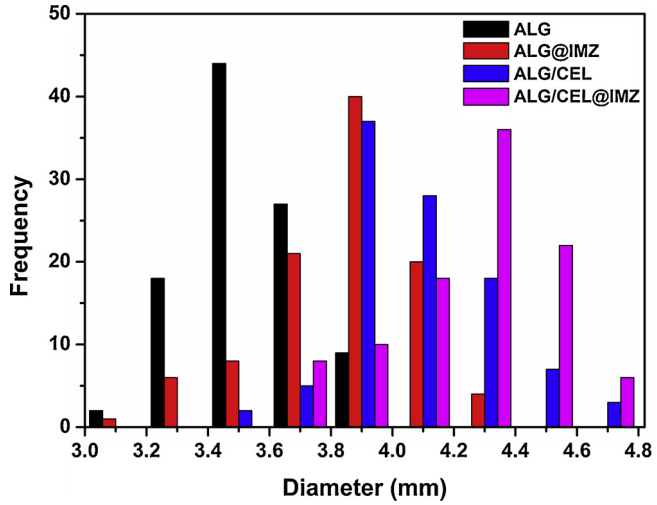

Fig. 5. Size distribution of ALG, ALG@IMZ, ALG/CEL, and ALG/CEL@IMZ beads.

those groups explains the increase of negative charges on the surface of the loaded beads and also indicates that the IMZ molecules are distributed through the bulk and surface regions of the beads corroborating the morphological analysis.

3.2. Swelling properties

In general lines, the controlled release of agrochemicals (i.e., herbicides, pesticides, nutrients, etc.) from swellable devices such as polysaccharide-based beads involves a diffusional and erosive process that is closely related to the liquid uptake capacity of such devices [40,41]. For this reason, to investigate this feature is paramount to designing an efficient IMZ carrier device. Here, the swelling behavior of ALG@IMZ and ALG/CEL@IMZ was investigated under different pH conditions, since the pH of the soil can vary as a function of several external and internal parameters. The pH of the swelling medium was varied from 5 to 7 to mimics the pH of the soils utilized in rice and soybean crops [42]. As aforementioned, IMZ has been utilized as an herbicide in these both crops.

The swelling capacity of the ALG@IMZ beads decreases with the increase of pH as shown in Fig. 5. At pH 5, the beads swelled fast achieving a swelling rate of ˜76% at the first 30 min. After that, the swelling rate slows down, and after 100 min, the liquid uptake tends to leave off, suggesting that the equilibrium was achieved. Under this pH condition, the maximum swelling was ˜93%. In contrast, close to neutrality (pH 6 and 7), the initial swelling rate (< 30 min) increased slower than at pH 5, which indicates that the swelling kinetics is attenuated under these pH conditions. Moreover, at pH 6 or 7, the swelling equilibrium was achieved fast (close to 30 min), and the maximum swelling rates were around 67% and 71%, respectively. Close to the neutrality, the negative charge density within the ALG network is higher due to the excess of deprotonated carboxylate groups of alginate, which can contribute to the electrostatic interaction between these

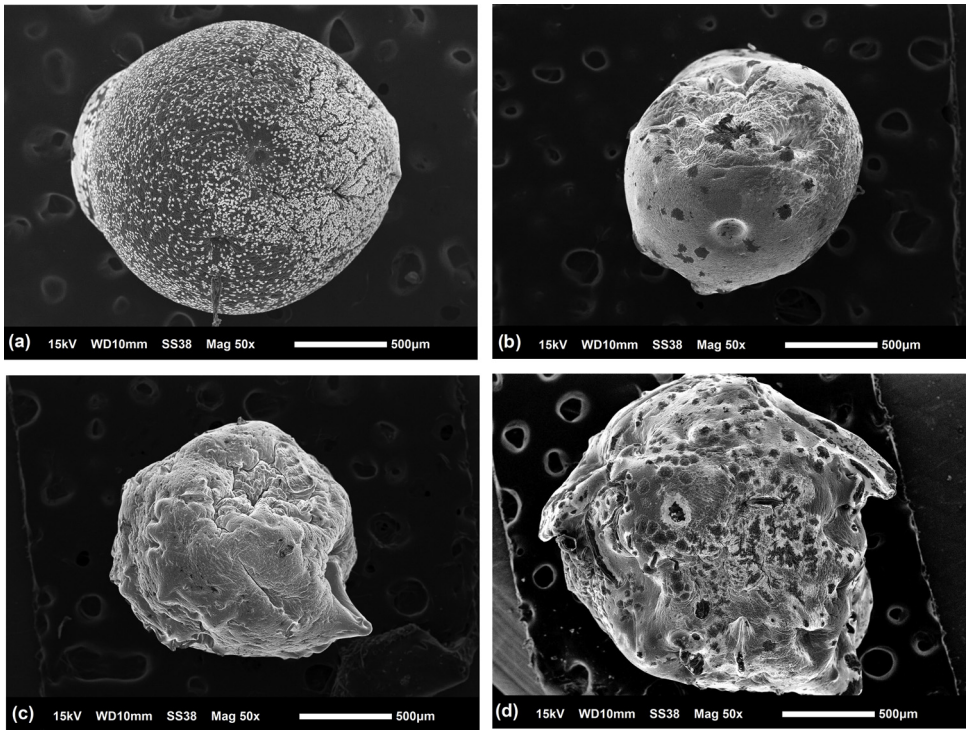

Fig. 6. SEM images of (a) ALG, (b) ALG@IMZ, (c) ALG/CEL, and (d) ALG/CEL@IMZ beads.

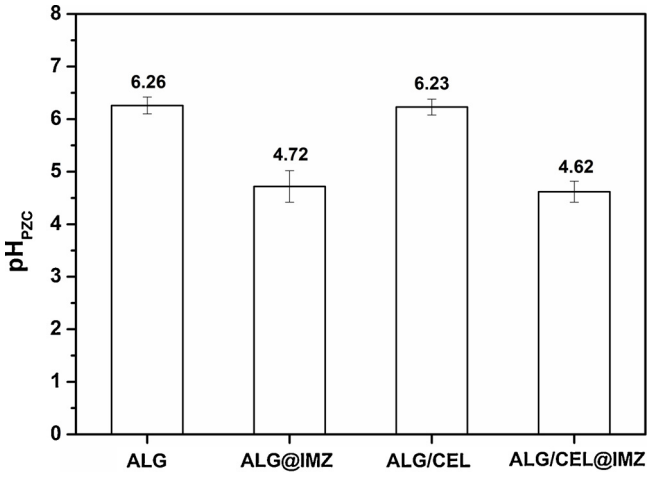

Fig. 7. pH_{PZC} values estimated for ALG, ALG@IMZ, ALG/CEL, and ALG/CEL@IMZ beads.

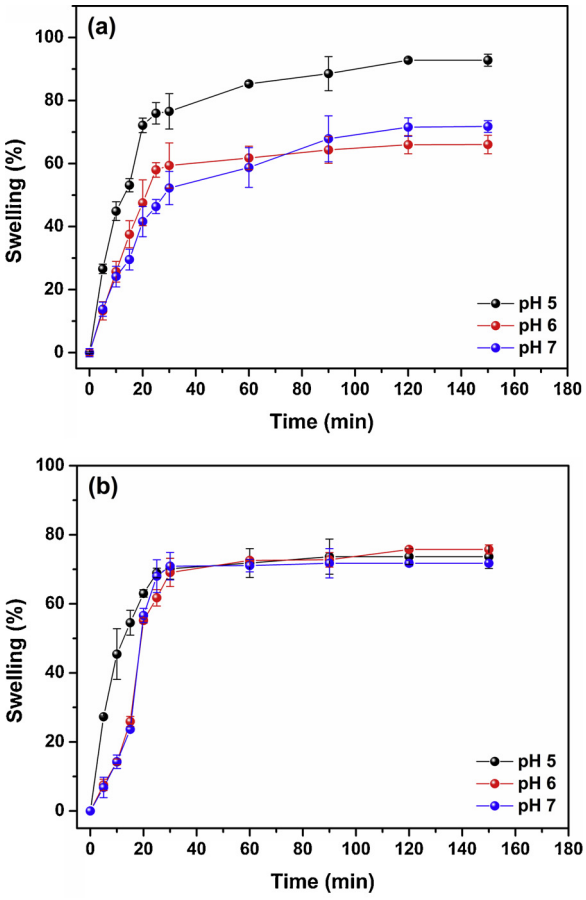

Fig. 8. Swelling profile of (a) ALG@IMZ and (b) ALG/CEL@IMZ beads under different pH conditions.

groups and Ca^{2+} ions. As a consequence, the bead network becomes more stable, preventing liquid sorption. Apart from this, the effect of pH on the swelling capacity of the ALG/CEL@IMZ was marginal, as observed in Fig. 8b. A minor remark regarding the initial swelling rates noticed for the samples swelled in pH 5, and pH 6 or 7 can be mentioned. For all tested pH conditions, the CEL-containing beads achieved the swelling equilibrium before the first 30 min, and the maximum swelling values were around 73%. The presence of CEL on the beads formulation attenuates the influence of the pH of the medium on the swelling capacity of the beads. This result suggests that CEL can be employed to prepare alginate-based beads with controllable swelling and releasing under this tested pH range.

Taking into account that the IMZ-carrier devices might be used under wet conditions due to the irrigation, for instance, the stability of the prepared beads (with and without IMZ) in aqueous medium was assessed. The degradability (%) of each sample after 4 weeks after

Table 2
Stability of the prepared beads after 4 weeks immersed in distilled water at room temperature.

Sample	Degradation (%)
ALG	75 ± 1
ALG@IMZ	68 ± 1
ALG/CEL	66 ± 2
ALG/CEL@IMZ	69 ± 1

immersion in distilled water (pH 6) is shown in Table 2. As noticed, the ALG beads presented the lowest stability since almost 75% of their initial weight was lost after the immersion period. On the other hand, the degradability assessed with other beads (ALG@IMZ, ALG/CEL, and ALG/CEL@IMZ) was statistically equal, and it remained lower than 68%. The degradability of this kind of beads can be associated with disruption of the electrostatic interactions among the alginate chains and the Ca^{2+} ions, which cause the beads dissolution. In parallel, the presence of IMZ and CEL into the ALG network reduced this process likely due to the secondary interactions that take place between alginate and IMZ/CEL (e.g., hydrogen bonding).

3.3. Release of IMZ from the ALG@IMZ and ALG/CEL@IMZ beads

The cumulative release of IMZ from the prepared beads (ALG@IMZ and ALG/CEL@IMZ) and the solubility profile of commercial IMZ are shown in (Fig. 9). As can be seen, more than 76% of IMZ are release from the commercial formulation in less than 1 day characterizing a typical burst release effect. The cumulative release of IMZ achieves 90% before the 3rd day, and maximum release is achieved on the 7th day of the experiment. In contrast, the cumulative release of IMZ from the polysaccharides-based beads exhibited a clear controlled profile over time (up to 30 days). For both carrier systems (ALG@IMZ and ALG/CEL@IMZ), the initial rate release was fast at the beginning of the experiment likely due to the release of the IMZ molecules encapsulated close to the surface of the bead. Later, the release rate slows down up to the end of the experiment. The presence of CEL within the ALG matrix affected the IMZ release profile, where the maximum cumulative release of IMZ was close to 37% for ALG/CEL@IMZ while this value was almost two folds higher (~70%) for ALG@IMZ. It is worth to note that despite the slow release rate presented by ALG@IMZ and ALG/CEL@IMZ even after 30 days of experiments the release curves depicted in Fig. 9 did not achieve the equilibrium, which means that the release of IMZ could remain for more extended periods for both encapsulating systems.

The mechanism associated with the IMZ release from the prepared

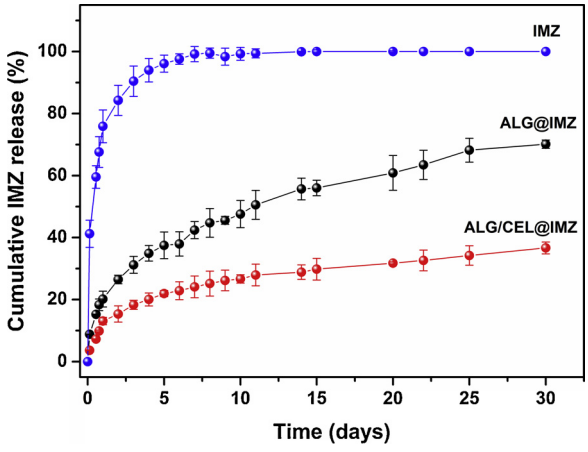

Fig. 9. Release profile of IMZ from commercial sample and from ALG@IMZ and ALG/CEL@IMZ beads as a function of time.

Table 3
Release rate constants of IMZ from the prepared beads.

Release model	Constants	ALG@IMZ	ALG/CEL@IMZ
Zero-order	k_0 (% day^{-1})	0.019	0.009
	R^2	0.870	0.781
First-order	k_1 (day^{-1})	0.051	0.049
	R^2	0.646	0.517
Hixson-Crowell	k_{HC} ($\%^{1/3}$ day^{-1})	0.012	0.008
	R^2	0.733	0.656
Korsmeyer-Peppas	k_{KP}	0.199	0.112
	n	0.38	0.40
	R^2	0.998	0.978
	$t_{0.5}$ (days)	11.30	43.73

beads was assessed by fitting the collected data with different mathematical models: Zero-order, first-order, Hixson-Crowell, and Korsmeyer-Peppas [43–45]. The equations of these mathematical models are listed in Table S1 (Supplementary material). The kinetic parameters, as well as the coefficients of determination (R^2) calculated from the models, are depicted in Table 3.

According to the data provided in Table 3, it is clear that the release data collected from both systems were better fitted by the Korsmeyer-Peppas model ($R^2 > 0.97$) (see Figs. S1a,b). This semi-empirical model encompasses the data analysis of Fickian and non-Fickian diffusional release from polymer-based carrier devices [46,47]. It is worth to say that this model works well for analyzing the first 60% of IMZ released [46]. The constant k_{KP} incorporates structural and geometric characteristics of the polymeric system and the encapsulated compound, while the n constant is denoted as the release exponent associated with the release mechanism. The values of k_{KP} calculated for ALG@IMZ and ALG/CEL@IMZ showed that the release of IMZ is slower for the beads containing CEL. It means that there is a stronger interaction between IMZ and this carrier device. The values of n calculated for ALG@IMZ and ALG/CEL@IMZ were close to 0.43, which indicates that for spherical devices, the release mechanism is driven by Fickian diffusion [46–48]. In this particular case, Fickian diffusion refers to the solute transport process in which the polymer relaxation time is much greater than the specific solvent diffusion time [47]. This release mechanism has been widely associated with polysaccharide-based devices used to encapsulate agrochemicals and drugs [48,49]. Another mathematical parameter that can be calculated from the Korsmeyer-Peppas model is the time necessary to release 50% of the initial amount of IMZ encapsulated within the prepared beads. This parameter (denoted as $t_{0.5}$) is calculated per Eq. (6):

$$t_{0.5} = \left(\frac{0.5}{k_{KP}}\right)^{1/n} \quad (6)$$

As can be seen in Table 3, the values of $t_{0.5}$ calculate for ALG@IMZ, and ALG/CEL@IMZ was 11.30 and 43.73 days, respectively. These results indicate that the incorporation of small amounts of CEL within the ALG network is an efficient strategy to slow the release of IMZ from the beads. It can be assumed that the CEL microfibers entrapped into the ALG network act as physical barriers against the IMZ diffusion outward the beads. This effect is called tortuosity, which in practical terms means that the CEL microfibers form cutting and tortuous pathways inside the ALG network slowing the IMZ release process [50,51] (see Fig. 10). Taken together, the results presented here allow inferring that the microparticles prepared from alginate and cellulose can be used as promising devices to the controlled and efficient release of IMZ.

4. Conclusion

In this study, alginate (ALG) and alginate/cellulose (ALG/CEL) beads were prepared through the ionic crosslinking of alginate chains by Ca^{2+} ions. Both beads systems were tested as vehicles for

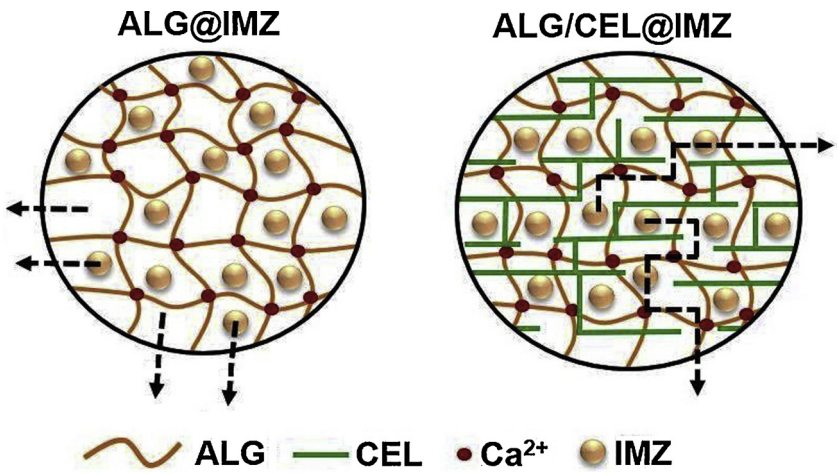

Fig. 10. Schematic illustration of release process of IMZ from ALG@IMZ and ALG/CEL@IMZ showing the tortuosity effect caused by the presence of CEL into the ALG network.

encapsulation and controlled delivery of imazethapyr (IMZ). As assessed, the presence of CEL into the beads increases the encapsulation efficiency of IMZ as compared to the pristine ALG beads. Analytical techniques performed here revealed that the IMZ molecules undergo a phase transition from crystalline to amorphous after the encapsulation. Moreover, slight interaction takes place between the IMZ and the beads matrices. The spherical beads exhibited some pH-dependent behavior regarding the liquid uptaking, which can be attenuated by the presence of CEL. Furthermore, IMZ and CEL increase the stability of ALG beads in water. Release experiments confirmed that both beads system could control and prolong the IMZ release up to 30 days. Different mathematical models fitted the release data, and the better results were ascribed to the Korsmeyer-Peppas model ($R^2 > 0.97$). The *n* values for the release of IMZ from ALG@IMZ and ALG/CEL@IMZ indicate that this process is driven by Fickian-diffusion mechanism. Also, the presence of CEL into the beads slower the release of IMZ likely due to its interaction with the IMZ molecules and, even, due to the tortuosity effect caused by the distribution of CEL microfibers into the ALG network. In conclusion, both beads systems (ALG and ALG/CEL) are useful to control the release of IMZ for prolonged periods providing an option for adjustment in herbicide usage in field conditions.

Declaration of Competing Interest

None.

Acknowledgments

The authors thank CNPq for their financial support (Universal grant. – Process 404744/2018-4). CNPq is also acknowledged for the fellowship to A.R.F. (Process 305974/2016-5). This study was financed in part by the Coordenação de Aperfeiçoamento de Pessoal de Nível Superior, Brazil (CAPES), Finance Code 001.

Appendix A. Supplementary data

Supplementary material related to this article can be found, in the online version, at doi:https://doi.org/10.1016/j.colsurfa.2019.123970.

References

[1] A.H.C. Van Bruggen, M.M. He, K. Shin, V. Mai, K.C. Jeong, M.R. Finckh, J.G. Morris, Environmental and health effects of the herbicide glyphosate, Sci. Total Environ. 616 (2018) 255–268.
[2] R.J. Kremer, Environmental implications of herbicide resistance: soil biology and ecology, Weed Sci. 62 (2014) 415–426.
[3] M.A. Marin-Morales, B.C. Ventura-Camargo, M.M. Hoshina, Toxicity of Herbicides: Impact on Aquatic and Soil Biota and Human Healthy, 1th ed., InTech, London, 2013, pp. 68–89.
[4] Y. El-Nahhal, S. Nir, L. Margulies, B. Rubin, Reduction of photodegradation and volatilization of herbicides in organo-clay formulations, Appl. Clay Sci. 14 (1999) 105–119.
[5] M.E. Taverna, C.A. Busatto, M.R. Lescano, V.V. Nicolau, C.S. Zalazar, G.R. Meira, D.A. Estenoz, Microparticles based on ionic and organosolv lignins for the controlled release of atrazine, J. Hazard. Mater. 359 (2018) 139–147.
[6] J.K. Norsworthy, S.M. Ward, D.R. Shaw, R.S. Llewellyn, R.L. Nichols, T.M. Webster, K.W. Bradley, G. Frisvold, S.B. Powles, N.R. Burgos, W.W. Witt, M. Barrett, Reducing the risks of herbicide resistance: best management practices and recommendations, Weed Sci. 60 (2012) 31–62.
[7] P. Wang, E. Lombi, F.J. Zhao, P.M. Kopittke, Nanotechnology: a new opportunity in plant sciences, Trend Plant Sci. 21 (2016) 699–712.
[8] F. Sopena, C. Maqueda, E. Morillo, Controlled release formulations of herbicides based on micro-encapsulation, Ciencia e Investigacion Agraria 36 (2009) 27–42.
[9] T. Undabeytia, E. Recio, C. Maqueda, E. Morillo, E. Gomez-Pantoja, T. Sanchez-Verdejo, Reduced metribuzin pollution with phosphatidylcholine-clay formulations, Pest Manag. Sci. 67 (2011) 271–278.
[10] S.F. Peteu, F. Oancea, O.A. Sicuia, F. Constantinescu, S. Dinu, Responsive polymers for crop protection, Polymers 2 (2010) 229–251.
[11] M.R. Guilherme, F.A. Aouada, A.R. Fajardo, A.F. Martins, A.T. Paulino, M.F.T. Davi, A.F. Rubira, E.C. Muniz, Superabsorbent hydrogels based on polysaccharides for application in agriculture as soil conditioner and nutrient carrier: a review, Eur. Polym. J. 72 (2015) 365–385.
[12] S.R. Nadendla, T.S. Rani, P.R. Vaikuntapu, R.R. Maddu, A.R. Podile, Harpin(Pss) encapsulation in chitosan nanoparticles for improved bioavailability and disease resistance in tomato, Carbohyd. Polym. 199 (2018) 11–19.
[13] S. Kumar, G. Bhanjana, A. Sharma, N. Dilbaghi, M.C. Sidhu, K.H. Kim, Development of nanoformulation approaches for the control of weeds, Sci. Total Environ. 586 (2017) 1272–1278.
[14] K. Wilpiszewska, T. Spychaj, W. Pazdzioch, Carboxymethyl starch/montmorillonite composite microparticles: properties and controlled release of isoproturon, Carbohyd. Polym. 136 (2016) 101–106.
[15] K.I. Draget, C. Taylor, Chemical, physical and biological properties of alginates and their biomedical implications, Food Hydrocoll. 25 (2011) 251–256.
[16] M. Fertah, A. Belfkira, E.M. Dahmane, M. Taourirte, F. Brouillette, Extraction and characterization of sodium alginate from Moroccan Laminaria digitata brown seaweed, Arab. J. Chem. 10 (2017) S3707–S3714.
[17] E.C. Mei, S.K. Li, J.W. Song, R.R. Xing, Z.M. Li, X.H. Yan, Self-assembling Collagen/Alginate hybrid hydrogels for combinatorial photothermal and immuno tumor therapy, Colloids Surf. A Physicochem. Eng. Asp. 577 (2019) 570–575.
[18] A. Rashidzadeh, A. Olad, M.J. Hejazi, Controlled release systems based on intercalated paraquat onto montmorillonite and clinoptilolite clays encapsulated with sodium alginate, Adv. Polym. Tech. 36 (2017) 177–185.
[19] S. Dubey, V. Jhelum, P.K. Patanjali, Controlled release agrochemicals formulations: a review, J. Sci. Ind. Res. 70 (2011) 105–112.
[20] B. Singh, D.K. Sharma, A. Dhiman, A. Gupta, Applications of natural polysaccharide-based beads for slow release herbicide formulation, Toxicol. Environ. Chem. 93 (2011) 616–622.
[21] D. Wang, A critical review of cellulose-based nanomaterials for water purification in industrial processes, Cellulose 26 (2019) 687–701.
[22] V. Kumar, A. Singh, T.K. Das, D.J. Sarkar, S.B. Singh, R. Dhaka, A. Kumar, Release behavior and bioefficacy of imazethapyr formulations based on biopolymeric hydrogels, J. Environ. Sci. Health B 52 (2017) 402–409.
[23] H.M. Brown, Mode of action, crop selectivity, and soil relations of the sulfonylurea herbicides, Pest. Sci. 29 (1990) 263–281.
[24] G.T. Voss, M.S. Gularte, A.G. Vogt, J.L. Giongo, R.A. Vaucher, J.V.Z. Echenique,

M.P. Soares, C. Luchese, E.A. Wilhelm, A.R. Fajardo, Polysaccharide-based film loaded with vitamin C and propolis: a promising device to accelerate diabetic wound healing, Int. J. Pharm. 552 (2018) 340–351.
[25] H.F. Sun, S.K. Li, W. Qi, R.R. Xing, Q.L. Zou, X.H. Yan, Stimuli-responsive nanoparticles based on co-assembly of naturally-occurring biomacromolecules for in vitro photodynamic therapy, Colloids Surf. A Physicochem. Eng. Asp. 538 (2018) 795–801.
[26] T. Mahmood, M.T. Saddique, A. Naeem, P. Westerhoff, S. Mustafa, A. Alum, Comparison of different methods for the point of zero charge determination of NiO, Ind. Eng. Chem. Res. 50 (2011) 10017–10023.
[27] H. Daemi, M. Barikani, Synthesis and characterization of calcium alginate nanoparticles, sodium homopolymannuronate salt and its calcium nanoparticles, Sci. Iran. 19 (2012) 2023–2028.
[28] W.P. Voo, B.B. Lee, A. Idris, A. Islam, B.T. Tey, E.S. Chan, Production of ultra-high concentration calcium alginate beads with prolonged dissolution profile, RSC Adv. 5 (2015) 36687–36695.
[29] E.F. Lessa, M.S. Gularte, E.S. Garcia, A.R. Fajardo, Orange waste: a valuable carbohydrate source for the development of beads with enhanced adsorption properties for cationic dyes, Carbohyd. Polym. 157 (2017) 660–668.
[30] P. Sundarrajan, P. Eswaran, A. Marimuthu, L.B. Subhadra, P. Kannaiyan, One pot synthesis and characterization of alginate stabilized semiconductor nanoparticles, Bull. Korean Chem. Soc. 33 (2012) 3218–3224.
[31] B. Benli, Effect of borax addition on the structural modification of bentonite in biodegradable alginate-based biocomposites, J. Appl. Polym. Sci. 128 (2013) 4172–4180.
[32] L. Li, Y. Fang, R. Vreeker, I. Appelqvist, E. Mendes, Reexamining the egg-box model in calcium-alginate gels with X-ray diffraction, Biomacromolecules 8 (2007) 464–468.
[33] S. Park, J.O. Baker, M.E. Himmel, P.A. Parilla, D.K. Johnson, Cellulose crystallinity index: measurement techniques and their impact on interpreting cellulase performance, Biotech. Biofuel 3 (2010) 1–10.
[34] A.I. Cernencu, A. Lungu, D. Dragusin, A. Serafim, E. Vasile, C. Ionescu, H. Iovu, Design of cellulose-alginate films using PEG/NaOH aqueous solution as co-solvent, Cellulose 24 (2017) 4419–4431.
[35] D. Kulig, A. Zimoch-Korzycka, A. Jarmoluk, K. Marycz, Study on alginate-chitosan complex formed with different polymers ratio, Polymers 8 (2016) 164–187.
[36] H.P. Yang, R. Yan, H.P. Chen, D.H. Lee, C.G. Zheng, Characteristics of hemicellulose, cellulose and lignin pyrolysis, Fuel 86 (2007) 1781–1788.
[37] P. Khazaeli, A. Pardakhty, F. Hassanzadeh, Formulation of ibuprofen beads by ionotropic gelation, Iran. J. Pharm. Res. 7 (2008) 163–170.
[38] W.T. Zhao, Y. Qi, Y. Wang, Y. Xue, P. Xu, Z.C. Li, Q. Li, Morphology and thermal properties of calcium alginate/reduced graphene oxide composites, Polymers 10 (2018) E990.
[39] R. Tazi, S. El Hasini, H. Khouja, S. Zaydoun, A. Zrinehl, M. El Azzouzi, Interactions of the aminotriazole and imazethapyr herbicides with humic acid extracted from moroccan soil, Res. J. Pharm. Biol. Chem. Sci. 6 (2015) 227–234.
[40] B.C. Zhong, S. Wang, H.H. Dong, Y.F. Luo, Z.X. Jia, X.Y. Zhou, M.Z. Chen, D. Xie, D.M. Jia, Halloysite tubes as nanocontainers for herbicide and its controlled release in biodegradable poly(vinyl alcohol)/starch film, J. Agr. Food Chem. 65 (2017) 10445–10451.
[41] M.C. Neri-Badang, S. Chakraborty, Carbohyd. Polym. As controlled release devices for pesticides, J. Carbohyd. Chem. 38 (2019) 67–85.
[42] T.R. Yu, Characteristics of soil acidity of paddy soils in relation to rice growth, in: R.J. Wright, V.C. Baligar, R.P. Murmann (Eds.), Plant-Soil Interactions at Low pH. Developments in Plant and Soil Sciences, Springer, Netherlands, 1991, pp. 107–112.
[43] Y. Fu, W.J. Kao, Drug release kinetics and transport mechanisms of non-degradable and degradable polymeric delivery systems, Expert Opin. Drug Deliv. 7 (2010) 429–444.
[44] A. Roy, S.K. Singh, J. Bajpai, A.K. Bajpai, Controlled pesticide release from biodegradable polymers, Central Eur. J Chem. 12 (2014) 453–469.
[45] Y.J. Sun, Y.L. Ma, G.Z. Fang, S.X. Ren, Y.J. Fu, Controlled pesticide release from porous composite hydrogels based on lignin and polyacrylic acid, Bioresources 11 (2016) 2361–2371.
[46] R.W. Korsmeyer, R. Gurny, E. Doelker, P. Buri, N.A. Peppas, Mechanisms of solute release from porous hydrophilic polymers, Int. J. Pharm. 15 (1983) 25–35.
[47] F.A. Aouada, M.R. de Moura, W.J. Orts, L.H.C. Mattoso, Polyacrylamide and methylcellulose hydrogel as delivery vehicle for the controlled release of paraquat pesticide, J. Mater. Sci. 45 (2010) 4977–4985.
[48] J.F. Li, Y.M. Li, H.P. Dong, Controlled release of herbicide acetochlor from clay/carboxylmethylcellulose gel formulations, J. Agric. Food Chem. 56 (2008) 1336–1342.
[49] J.H. Lee, Y. Yeo, Controlled drug release from pharmaceutical nanocarriers, Chem. Eng. Sci. 125 (2015) 75–84.
[50] E.T. Tenorio-Neto, D.D.S. Lima, M.R. Guilherme, M.K. Lima-Tenorio, D.B. Scariot, C.V. Nakamura, M.H. Kunita, A.F. Rubira, Synthesis and drug release profile of a dualresponsive poly(ethylene glycol) hydrogel nanocomposite, RSC Adv. 7 (2017) 27637–27644.
[51] S.A. Paralikara, J. Simonsen, J. Lombardi, Poly(vinyl alcohol)/cellulose nanocrystal barrier membranes, J. Membrane Sci. 320 (2008) 248–258.